4-hydroxytamoxifen leads to PrPSc clearance by conveying both PrPC and PrPSc to lysosomes independently of autophagy.

Ludovica Marzo, Zrinka Marijanovic, Duncan Browman, Zeina Chamoun, Anna Caputo, Chiara Zurzolo

4-hydroxytamoxifen leads to PrP^{Sc} clearance by conveying both PrP^{C} and PrP^{Sc} to lysosomes independently of autophagy

Ludovica Marzo[1,2,*], Zrinka Marijanovic[1,*], Duncan Browman[1], Zeina Chamoun[1], Anna Caputo[1] and Chiara Zurzolo[1,2,‡]

[1]Institut Pasteur, Unité de Trafic Membranaire et Pathogenèse, 25 rue du Docteur Roux, 75015 Paris, France
[2]Dipartimento di Biologia e Patologia Cellulare e Molecolare, Università di Napoli 'Federico II', Via Pansini 5, 80131 Napoli, Italy

*These authors contributed equally to this work
‡Author for correspondence (chiara.zurzolo@pasteur.fr)

Accepted 2 January 2013
Journal of Cell Science 126, 1345–1354

doi: 10.1242/jcs.114801

Summary

Prion diseases are fatal neurodegenerative disorders involving the abnormal folding of a native cellular protein, named PrP^{C}, to a malconformed aggregation-prone state, enriched in beta sheet secondary structure, denoted PrP^{Sc}. Recently, autophagy has garnered considerable attention as a cellular process with the potential to counteract neurodegenerative diseases of protein aggregation such as Alzheimer's disease, Huntington's disease, and Parkinson's disease. Stimulation of autophagy by chemical compounds has also been shown to reduce PrP^{Sc} in infected neuronal cells and prolong survival times in mouse models. Consistent with previous reports, we demonstrate that autophagic flux is increased in chronically infected cells. However, in contrast to recent findings we show that autophagy does not cause a reduction in scrapie burden. We report that in infected neuronal cells different compounds known to stimulate autophagy are ineffective in increasing autophagic flux and in reducing PrP^{Sc}. We further demonstrate that tamoxifen and its metabolite 4-hydroxytamoxifen lead to prion degradation in an autophagy-independent manner by diverting the trafficking of both PrP and cholesterol to lysosomes. Our data indicate that tamoxifen, a well-characterized, widely available pharmaceutical, may have applications in the therapy of prion diseases.

Key words: PrP^{Sc}, TAM, OHT, Autophagy, Lysosomal Degradation, Cholesterol

Introduction

Transmissible spongiform encephalopathies are infectious, neurodegenerative diseases involving the abnormal folding of the cellular prion protein PrP^{C} into a pathological conformer PrP^{Sc}. This malconformed state also leads to its accumulation as aggregates in both the cytoplasm of affected neurons and the interstitial spaces within the brains of afflicted individuals (Prusiner, 1998).

Recently, macroautophagy has been described as an important process in the pathogenesis of neurodegenerative diseases involving protein aggregation such as Alzheimer's, Huntington's and Parkinson's disease, as well as in prion diseases (Cherra et al., 2010). As post-mitotic cells that must endure for the lifetime of an organism, neurons require efficient mechanisms to avoid accumulating toxic protein aggregates. It has been proposed that macroautophagy, often referred to simply as 'autophagy', is one such mechanism (Rubinsztein et al., 2007; Wong and Cuervo, 2010). Recent evidence suggests that dysfunction in the autophagic pathway is common to many neurodegenerative diseases (Wong and Cuervo, 2010). Furthermore, mice engineered for neuron-specific knockout of the essential autophagy genes *Atg5* or *Atg7* have a neurodegenerative phenotype accompanied by massive protein aggregate accumulation and resulting inexorably in death within the first few months of birth (Hara et al., 2006; Komatsu et al., 2006). Moreover, upregulation of autophagy was shown to efficiently counteract neurodegeneration in both *in vitro* and *in vivo* models (Wong and Cuervo, 2010).

The role of autophagy in prion diseases is highly debated (Heiseke et al., 2010). Autophagic vacuoles were first detected in neuronal cell models chronically infected with prions (Schätzl et al., 1997). More recently, autophagic vacuoles were identified in synapses in various forms of human prion disease (Sikorska et al., 2004) and it was found that they formed in neuronal perikarya, neurites and synapses in experimentally induced scrapie, Creutzfeldt–Jakob disease (CJD) and Gerstmann–Sträussler–Scheinker (GSS) syndrome (Liberski et al., 2008). Therefore, it was proposed that autophagy could play a disease-promoting role by contributing to the formation of spongiform encephalopathies (Liberski et al., 2008; Liberski and Jeffrey, 2004). In addition, it has been demonstrated that a number of autophagy-inducing compounds such as lithium salts, trehalose and rapamycin are effective in reducing PrP^{Sc} burden in cultured neuroblastoma cells (N2a) and delay the onset of symptoms in prion-infected mice in prophylactic treatment models (Aguib et al., 2009; Heiseke et al., 2009). Thus, induction of autophagy was proposed as a novel approach for the treatment of prion diseases.

However, a more systematic analysis of the role of autophagy in prion infection is needed because the molecular mechanisms by which autophagy could be protective are still not understood. In particular it has to be considered that the majority of PrP^{Sc} resides

in the endocytic pathway and not in the cytosol (Campana et al., 2005; Caughey et al., 2009). The availability of new tools and recent advances in the understanding of the dynamic process of autophagic flux prompted us to re-examine the role of autophagy in prion propagation, trafficking and clearance. We observed a basal activation of autophagy in all neuronal cell models examined. Of interest, chronic scrapie infection results in an increase in autophagic flux, which does not lead to any significant colocalisation of PrP^{Sc} with autophagic vacuoles. We also report that autophagic flux could not be further stimulated by autophagy-inducing compounds such as rapamycin, previously shown to clear prion-infection in scN2a cells (Aguib et al., 2009; Heiseke et al., 2009). Consistently, we demonstrated that tamoxifen (TAM) and its active metabolite, 4-hydroxytamoxifen (OHT), which were previously shown to stimulate autophagy, enhance PrP^{Sc} degradation in lysosomes by relocating PrP^{C}, PrP^{Sc} and cholesterol, into lysosomes in an autophagy-independent manner.

Results

Chronic prion infection induces autophagic flux in neuronal cell culture models

To investigate the role of autophagy in PrP^{Sc} metabolism, we analysed whether scrapie infection could affect autophagic flux in neuronal cell lines by comparing uninfected and chronically infected GT1 and N2a cells (respectively, GT1 and scGT1, and N2a and ScN2a cells), using both fluorescence microscopy and biochemical approaches. To monitor potential changes in autophagic flux, we analysed LC3, a well-known autophagic marker protein specifically associated with autophagosome membranes (Kabeya et al., 2000). In order to measure the dynamic flux of the autophagy pathway from early autophagosomes through to late autolysosomes, we used the tandem fluorescently tagged LC3 construct (tfLC3, encoding for LC3 linked to both GFP and RFP proteins) combined with inhibition of lysosomal proteases in both control and infected cells. This tool is based on the differential sensitivity of GFP and RFP fluorophores to the acidic pH of lysosomes and is specifically used to monitor the progression of autophagy (Klionsky et al., 2008). Although both GFP and RFP signals are observable in autophagosomes, following the maturation process to phagolysosomes only the RFP signal remains because of the selective quenching of the GFP-linked molecule (Kimura et al., 2009).

Quantification of labelled vesicles in control GT1 cells transfected with tfLC3 revealed that 55% of the vesicles were double-positive autophagosomes and 45% were red-only autolysosomes. In control N2a cells, 35% of the vesicles were double-positive autophagosomes, whereas 65% of the vesicles were red-only autolysosomes (Fig. 1A–D). Thus, using this improved tool to measure autophagic flux, a basal activation of the autophagic pathway was detected in both neuronal cell lines, in contrast to previous reports in which autophagy was not detected in N2a cells (Aguib et al., 2009; Heiseke et al., 2009) (see Discussion). Of interest, quantification of the red-only positive vesicles revealed a substantial increase in the number of autolysosomes in both infected cells lines. Specifically, the percentage of red-only autolysosomes in infected scGT1 and scN2a cells rose from 45% to 60% and from 65% to 90%, respectively, of all LC3-decorated vesicles (Fig. 1A–D). These data suggest that autophagic flux is increased above the basal level under conditions of chronic scrapie infection in neuronal cells. Consistently, the average number of LC3-positive vesicles per cell also increased upon infection (data not shown; supplementary material Fig. S1A,B).

These results were corroborated by western blot analysis comparing the endogenous levels of LC3-II in infected and non-infected cells, in the presence or absence of lysosomal protease inhibitors (Fig. 1E). LC3-II is the post-translationally modified

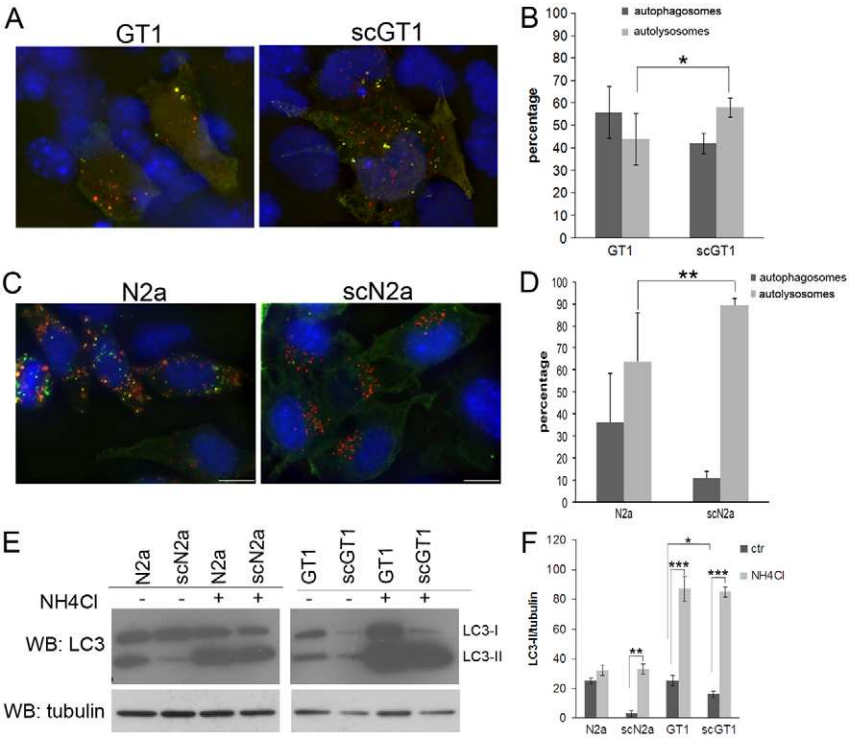

Fig. 1. Autophagic flux in non-infected and prion-infected GT1 and N2a cells. (**A**,**C**) Both non-infected and infected GT1 and N2a cells were transfected with the Tf-LC3 construct and analysed by fluorescence microscopy. LC3-positive vesicles indicate activation of autophagy (both green and red labelling); appearance of red-only puncta indicate progression of autophagic flux. Scale bars: 10 μm; (**B**,**D**) Quantification of the results from A and C presented as the percentage of both green and red (autophagosomes) and red-only vesicles (autolysosomes) per cell (means ± s.e.m., $n=3$); *$P<0.05$, **$P<0.01$. (**E**,**F**) Endogenous levels of LC3-II in infected and non-infected cells treated (+) or not (−) with lysosomal inhibitors, revealed by monoclonal anti-LC3 antibody (clone 2G6) on western blots (values are means ± s.e.m., $n=3$); *$P<0.05$, **$P<0.01$, ***$P<0.001$. Quantified results were normalized to tubulin levels. Note that both fluorescence microscopy and a biochemical approach confirmed an activation of autophagic flux during prion infection in both cell lines.

form of LC3, associated with autophagosome membranes, and can be distinguished from its precursor LC3-I by its increased electrophoretic mobility in SDS-PAGE (16 kDa for LC3-I versus 14 kDa for LC3-II) (Kabeya et al., 2000). Treatment with lysosomal protease inhibitors partially inhibits the degradation of LC3-II delivered to lysosomes during organelle fusion, thus facilitating its recovery and therefore the assessment of the state of autophagic flux in a given condition (Kimura et al., 2009). As expected, we found a significant increase in the amount of LC3-II upon ammonium chloride treatment in both scGT1 and scN2a cells (Fig. 1F). Importantly, this increase was greater in the infected cells compared to uninfected GT1 and N2a cells consistent with a higher rate of autophagic flux during prion infection (Fig. 1A–D).

To further corroborate our findings we analysed autophagic flux in CAD cells, another neuronal cell line capable of propagating prions (Gousset et al., 2009; Marijanovic et al., 2009). A comparable increase in both autophagic flux and average total number of LC3-positive vesicles per cell was observed in infected scCAD cells (supplementary material Fig. S1A,B) confirming that autophagy is activated in chronically infected cells.

In order to gain some insight into the mechanism and timing of this activation, we analysed whether *de novo* prion infection could modulate autophagy. We performed a live-cell imaging experiment in which we followed in real-time the fate of newly taken-up PrP^{Sc} aggregates, and simultaneously monitored the autophagic flux. CAD cells transfected with GFP-tagged LC3 (GFP–LC3) were challenged with Alexa-Fluor-546–PrP^{Sc}, a fluorescent infectious scrapie preparation (Gousset et al., 2009), and followed by live microscopy for up to 12 hours post-infection. Similar to chronically infected cells, autophagy was induced upon the uptake of Alexa-Fluor-546–PrP^{Sc} cells, as shown by the appearance of GFP–LC3 puncta. However, Alexa-Fluor-546–PrP^{Sc}-positive vesicles were clearly distinguished from LC3-positive autophagosomes (supplementary material Movies 1–3), suggesting that PrP^{Sc} was not being trafficked through the autophagic pathway.

Autophagy does not play a major role in PrP^{Sc} metabolism

The evidence indicating that autophagy was activated both in permanently and newly infected cells raised the question as to whether autophagy was involved in scrapie clearance. It was previously reported that treatment of infected scN2a cells with autophagy inducers (e.g. rapamycin, lithium or trehalose) decreased PrP^{Sc} levels in cells and delayed the course of disease in scrapie-infected mice, although with high variability (Aguib et al., 2009; Heiseke et al., 2009).

The presence of high levels of PrP^{Sc}, in spite of increased autophagic flux in permanently infected cells, along with our observations using fluorescent microscopy in newly infected cells (supplementary material Movies 1–3) suggested that either PrP^{Sc} was not being processed by the autophagic route or that this process was inefficient in reducing scrapie burden. Therefore, to directly test these hypotheses we monitored PrP^{Sc} levels following chemical stimulation of autophagy. Specifically, scGT1 and scN2a cells were treated for 5 days with either rapamycin, TAM or OHT, previously shown to induce autophagy (Klionsky and Emr, 2000; de Medina et al., 2009). Next, the levels of total PrP and proteinase K (PK)-resistant PrP were examined by limited proteinase K digestion and western blotting (Schätzl et al., 1997) to test the ability of these drugs to reduce PrP^{Sc} (Fig. 2A,C). Interestingly, whereas rapamycin, a well-known inducer of autophagy, caused only a moderate and not very consistent (see also Fig. 4) decrease in the PrP^{Sc} fraction (10–20%) in both cell lines (Fig. 2B,D), we found that TAM and particularly its metabolite OHT, were very efficient in PrP^{Sc} clearance (80–90%).

To understand whether PrP^{Sc} degradation was occurring in autophagic vacuoles we performed quantitative immunofluorescence after guanidine hydrochloride (GND) treatment (Marijanovic et al., 2009) to measure the

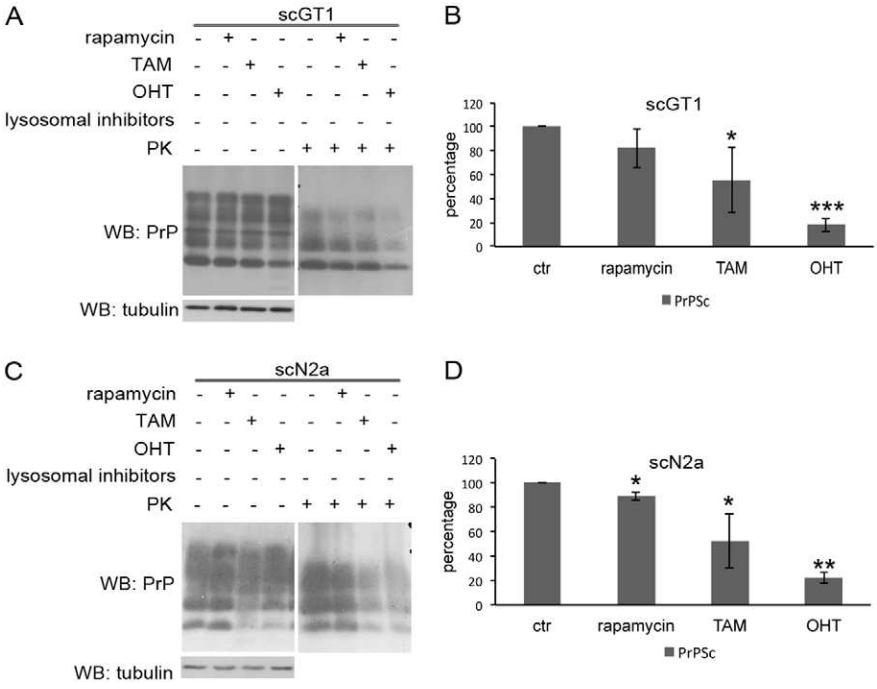

Fig. 2. Treatment with TAM and OHT is able to reduce PrP^{Sc} levels in both scGT1 and scN2a cells. (**A**,**C**) scGT1 and scN2a cells were treated with the different compounds for 5 days and levels of PrP^{Sc} (PK+) and total PrP (PK−) were detected on western blots by using Sha31 anti-PrP antibody. Tubulin was used as a control for equal loading. (**B**,**D**) Quantification of PrP^{Sc} levels after different treatments, presented as percentages of the level in untreated cells, which was considered to be 100% (values are means ± s.e.m., $n=3$); *$P<0.05$, **$P<0.001$, ***$P<0.0001$.

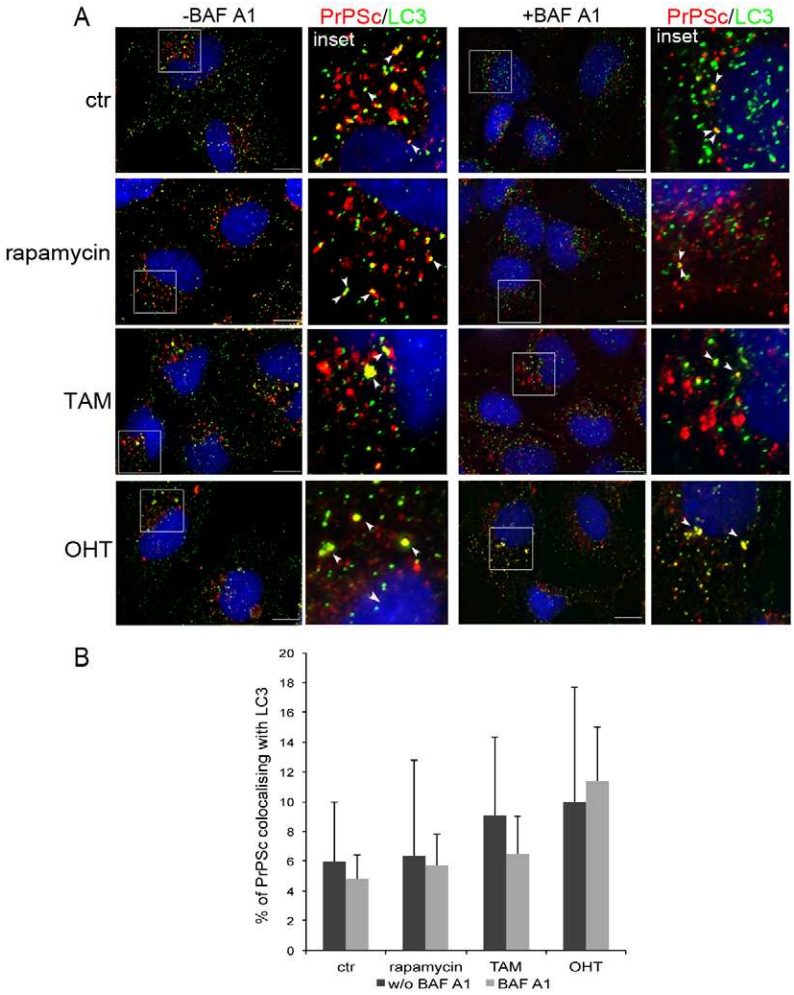

Fig. 3. PrP^{Sc} in autophagosomes does not change upon different treatments in scGT1 cells. (**A**) scGT1 cells were treated for 3 days with either rapamycin, TAM and OHT in the presence (+) or absence (−) of 100 µM Bafilomycin A1 and then subjected to double immunofluorescence analysis with a polyclonal anti-LC3 antibody and Saf32 anti-prion monoclonal antibody. 6 M guanidine hydrochloride treatment prior immunolabelling was used to reveal PrP^{Sc} epitopes. Colocalisation between PrP^{Sc} (in red)- and LC3 (green)-positive vesicles is shown in yellow. Scale bars: 10 µm. 'Insets' are enlarged images of the boxed areas. (**B**) Quantification of the colocalisation of the total PrP^{Sc} signal with autophagosomes (values are means ± s.e.m., $n=50$). Note that only a minor fraction of PrP^{Sc} was found in LC3-positive vesicles and both different treatments and lysosomal proteases inhibition did not increase its presence in these organelles (not statistically significant, $P>0.05$).

colocalisation of PrP^{Sc} and LC3-decorated vesicles, both in control cells and after the different drug treatments. Of interest, only a minor fraction of PrP^{Sc} (6%) colocalised with endogenous LC3 in permanently infected scGT1 cells (Fig. 3A,B). Furthermore, the amount of PrP^{Sc} in LC3-positive vesicles did not significantly increase upon rapamycin, TAM or OHT treatments (Fig. 3B). Similar results were obtained in scCAD cells (supplementary material Fig. S1E,F). To rule out fast lysosomal degradation as a possible cause for the lack of PrP^{Sc} localisation in LC3-positive autolysosomes we blocked the activity of lysosomal proteases using Bafilomycin A1 (Fig. 3A). However, despite this treatment, we could not observe any statistically significant increase of PrP^{Sc} in autophagic vesicles in scGT1 cells (Fig. 3B). These results support the hypothesis that the reduction in PrP^{Sc} observed upon TAM and OHT treatment does not occur through the autophagic pathway.

In order to directly rule out the involvement of autophagy in PrP^{Sc} degradation, which was reproducibly induced by these drugs, we used an RNAi approach. To this aim, we challenged scGT1 cells with siRNA targeting *Atg7*, an essential autophagic gene, in two subsequent rounds of transfection in order to maintain low levels of Atg7 during a 5-day treatment with rapamycin, TAM or OHT. In these conditions, upon 90% downregulation of Atg7 and LC3II reduction (Fig. 4A), rapamycin treatment did not give a consistent reduction of PrP^{Sc} (see quantification Fig. 4B). However, it was striking that both TAM and to a greater extent OHT treatments were still capable of decreasing PrP^{Sc} levels. Indeed, the magnitude of the TAM- and OHT-mediated decrease of scrapie in Atg7-depleted cells was indistinguishable from that of cells co-treated with scrambled control siRNA (Fig. 4B). Moreover, evidence from this experiment arguing against a role for autophagy in prion degradation was that no increase in PrP^{Sc} was observed in infected cells even after prolonged treatment with Atg7 siRNA alone (Fig. 4A, lanes 1 and 5 of the PK-treated extracts).

By measuring the ratio of autophagosomes and autolysosomes and LC3-II levels (supplementary material Fig. S2) we also found that none of these drugs was able to increase the autophagic flux beyond the high levels already observed in infected cells. However, it should be noted that unlike rapamycin, OHT treatment combined with lysosomal inhibitors did not increase LC3 II levels, suggesting an inhibition of autophagic flux in this condition (supplementary material Fig. S2). Similar results were obtained after 4-hour treatment, thus ruling out a possible cell adaptation to the 5-days treatment (supplementary material Fig. S3A). Nonetheless it should be noted that autophagy was induced by cell starvation in serum-reduced conditions (supplementary material Fig. S3A). The fact that the autophagic flux was not further increased by known autophagic inducers (rapamycin,

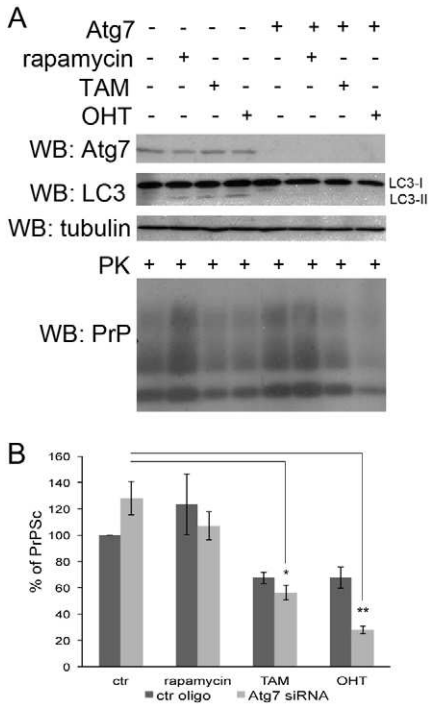

Fig. 4. Atg7 downregulation in scGT1 cells does not block PrP^{Sc} clearance upon rapamycin, TAM and OHT treatment. (**A**) scGT1 cells transfected with either control oligo (ctr oligo) or siRNA for Atg7 were treated for 5 days with rapamycin, TAM and OHT and then lysed. Atg7, LC3-II and total PrP levels were analysed by western blotting; tubulin was used as a control for equal loading. Cell lysates were treated with Proteinase K in order to measure PrP^{Sc} levels (PK+). (**B**) Quantification of the results from A, presented as the percentage of total PrP^{Sc} signal in untreated cells transfected with ctr oligo. Differences compared with levels of PrP^{Sc} signal in Atg7-siRNA-treated control cells (values are means ± s.e.m., $n=3$); $^{*}P<0.05$, $^{**}P<0.01$.

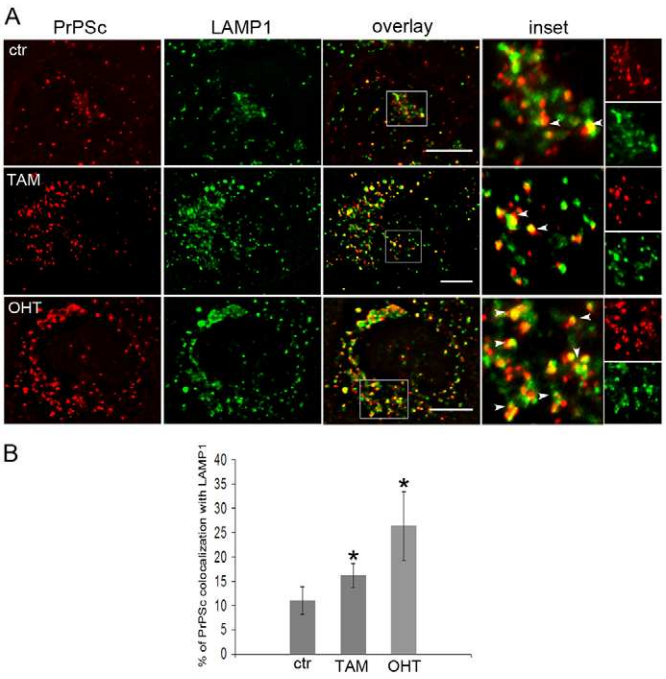

Fig. 5. PrP^{Sc} localisation in lysosomes increases upon OHT treatment. (**A**) Differences in PrP^{Sc} fraction in lysosomes were examined. scGT1 cells were treated for 3 days with either rapamycin, TAM and OHT and then subjected to double immunofluorescence analysis with anti-LAMP1 antibody (to stain lysosomes; green) and Saf32 anti-prion monoclonal antibody (after 6 M guanidine hydrochloride treatment to reveal PrP^{Sc}; red). 'Insets' are enlarged images of the boxes areas. (**B**) Quantification of the results from A, presented as the percentage of the total PrP^{Sc} signal colocalising with lysosomes. Differences compared with levels of PrP^{Sc} colocalising with lysosomes in control conditions (values are means ± s.e.m., $n=50$); $^{*}P<0.05$. Scale bars: 10 μm. Also, single-colour images of the insets are provided.

TAM and OHT) raised the question of whether these drugs were at all able to induce autophagy in our cell systems. Therefore, we measured the levels of p62 and LC3, two independent autophagy markers, in non-infected GT1 cells. Interestingly, we found that although rapamycin treatment was able to reduce the level of p62 treatment, TAM and OHT did not (supplementary material Fig. S3B). Consistently the ratio between LC3II and LC3 increased only upon rapamycin treatment but not after TAM and OHT stimulation (supplementary material Fig. S3C). These data indicate that rapamycin is able to induce authophagy in GT1 cells, but TAM and OHT are not, contrary to what had been shown in other cell types (Qadir et al., 2008; Samaddar et al., 2008). Combined with the observation that PrPSc degradation is enhanced upon TAM and OHT treatments but is not affected upon rapamycin addition (Fig. 2), our results clearly indicate that autophagy does not play a major role in PrP^{Sc} degradation and that TAM and OHT are potent prion-reducing agents in an autophagy-independent manner.

OHT and TAM causes redistribution of PrP^{Sc}, PrP^{C} and cholesterol to lysosomes

In order to understand how TAM and OHT induce PrP^{Sc} clearance in infected cells we examined whether these treatments would enhance PrP^{Sc} degradation in lysosomes, which represent the major degradative pathway for PrP^{Sc} (Shyng et al., 1993; Sunyach et al., 2003; Marijanovic et al., 2009). To this aim we quantified the amount of PrP^{Sc} present in lysosomes in control cells versus TAM- and OHT-treated cells. Specifically, scGT1 cells were treated with either TAM or OHT for 3 days and, after fixation, permeabilisation and GND treatment, the samples were immunostained for PrP^{Sc} and LAMP1, and the percentage of colocalisation between the two was evaluated (Fig. 5). Quantification of the two signals revealed that PrP^{Sc} was substantially enriched in lysosomes in TAM- and OHT-treated cells compared to untreated cells. OHT proved to be the more potent of the two, with treatment resulting in around 30% of PrP^{Sc} colocalising with LAMP1 compared with the 10% observed in the untreated cells (Fig. 5B). This result supports the involvement of lysosomal proteases in the degradation of PrP^{Sc} induced by these drugs treatments.

To examine this further, lysosomal degradation was inhibited using NH_4Cl and the effect on PrP^{Sc} levels in OHT-treated cells was analysed by western blotting (Fig. 6). We reasoned that if the observed decrease in PrP^{Sc} levels induced by OHT treatment was due to lysosomal degradation, inhibition of this process should restore PrP^{Sc} levels. Accordingly, we were able to show that treatment with NH_4Cl led to an increase in the PrP^{Sc} fraction and prevented the clearance induced by OHT (Fig. 6). Because PrP^{Sc} failed to accumulate in LC3-positive structures even in the

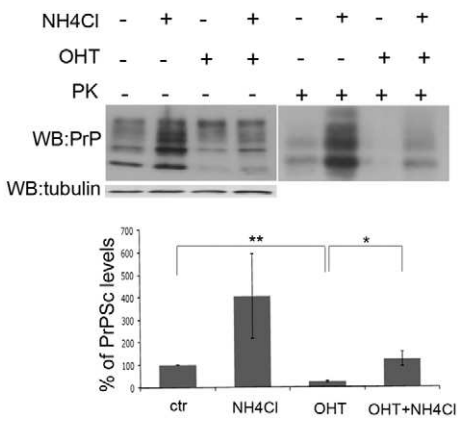

Fig. 6. PrP^{Sc} is degraded in lysosomes upon OHT treatment. scGT1 cells were treated for 5 days with OHT in presence (+) or absence (−) of NH_4Cl. PrP^{Sc} (PK+) and total PrP (PK−) were analysed by western blotting. Tubulin was used as a control for equal loading. Quantification of PrP^{Sc} levels are presented as a percentage of the level in untreated cells, which was considered to be 100% (values are means ± s.e.m., $n=3$). Note that lysosomal proteases inhibition counteracts the effect of OHT treatment restoring PrP^{Sc} levels. Differences compared with levels of PrP^{Sc} signal in control and OHT-treated cells, $*P<0.05$, $**P<0.01$.

context of lysosomal protease inhibition (Fig. 3), together these data indicate that TAM and OHT intensified PrP^{Sc} trafficking and degradation into lysosomes in an autophagy-independent manner.

Because the measured PrP^{Sc} results from a balance between the pathological conversion of PrP^{C} and degradation of PrP^{Sc} we also measured the fraction of PrP^{C} in lysosomes in control and OHT-treated scGT1 cells. In the control condition PrP^{C} is mainly restricted to the Golgi area and early/recycling endosomes, as previously shown by Marijanovic et al., but upon OHT treatment it redistributes to discrete vesicles colocalising with the lysosomal marker LAMP1 (Fig. 7) (Marijanovic et al., 2009). We found that upon OHT treatment 24% of PrP^{C} colocalised with LAMP1 compared with only 12% colocalisation in the no-drug control (Fig. 7). This suggests that OHT also perturbs the trafficking of PrP^{C}, the substrate of the PrP^{Sc} conversion, by redirecting it to lysosomes for degradation.

Although the above data showed that TAM and OHT induce prion degradation through enhanced lysosomal trafficking and degradation, the question remained as to which mechanism determines the increased accumulation of both PrP^{Sc} and PrP^{C} in lysosomes.

Several lines of *in vivo* and *in vitro* evidence have shown that both PrP^{C} and PrP^{Sc} have a high affinity for membrane domains enriched in cholesterol (Critchley et al., 2004; Galvan et al., 2005; Marijanovic et al., 2009) and that cholesterol levels regulate the distribution of PrP^{C} in different membrane domains (dendrites versus axons) in primary neurons (Galvan et al., 2005). Furthermore, TAM and OHT have been shown to perturb cholesterol homeostasis and trafficking in different cancer cell types (Suárez et al., 2004; de Medina et al., 2004; de Medina et al., 2011). Importantly, TAM has been shown to inhibit the exit of cholesterol from lysosomes leading to the accumulation of cholesterol-laden late endosomes/lysosomes (Suárez et al., 2004). If this also occurs in prion-infected neuronal cells a mechanistic explanation of our findings would be that an increase of cholesterol in lysosomes may result in the relocalisation of both PrP^{C} and PrP^{Sc} into these organelles.

In order to test this proposal we examined cholesterol distribution by filipin staining in TAM- and OHT-treated cells compared to untreated scGT1 cells. It was found that in contrast to the diffuse filipin staining observed in untreated cells, and in conditions where autophagy is induced (rapamycin-treated and starved cells), both TAM and OHT treatments resulted in a punctate staining pattern, partially colocalising with LAMP1 (Fig. 8), suggesting a redistribution of cholesterol and enrichment in lysosomes. The same phenomenon was observed in control uninfected cells (supplementary material Fig. S4). Noticeably, vesicles positive for both LAMP1 and filipin did not colocalise extensively with LC3, thus supporting the evidence that cholesterol-enriched lysosomes do not result from induction of autophagy (supplementary material Fig. S4). Importantly, the

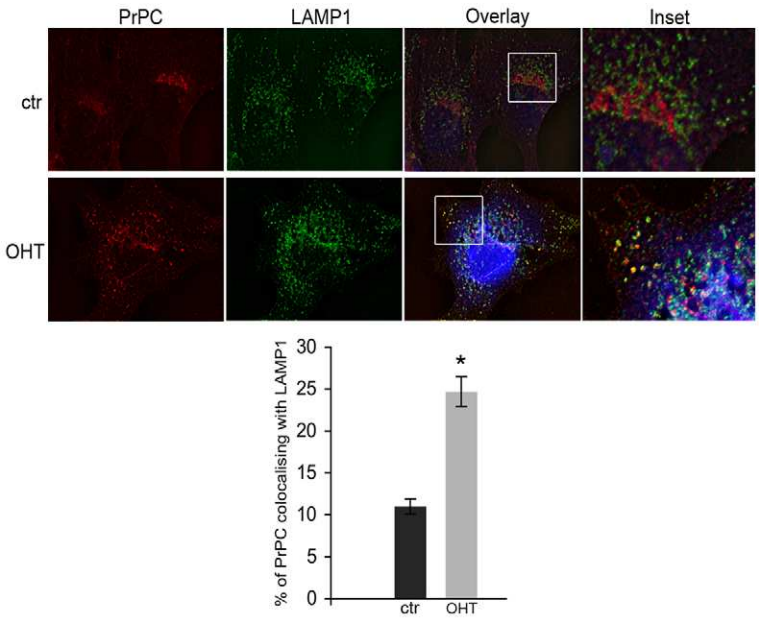

Fig. 7. Upon OHT treatment a fraction of PrP^{C} relocates to lysosomes in scGT1 cells. The presence of PrP^{C} in lysosomes was evaluated. scGT1 cells were treated for 3 days with OHT and then subjected to a double immunofluorescence assay with anti-LAMP1 antibody (to stain lysosomes; green) and Sha31 anti-PrP monoclonal antibody (after guanidine hydrochloride treatment to reveal PrP^{Sc} epitopes; red). Note that in control untreated cells PrP^{C} is mainly distributed in the Golgi compartment, early and recycling endosomes, but upon OHT treatment it partially relocated to lysosomes, as indicated by a more scattered signal and the quantitative colocalisation analysis. Quantification of the percentage of total PrP^{C} signal colocalising with lysosomes (values are means ± s.e.m., $n=50$); $*P<0.0001$.

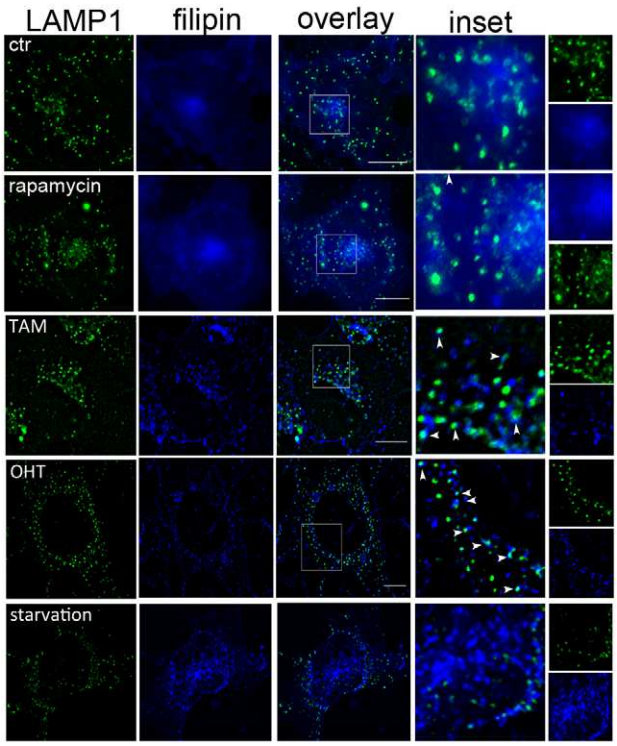

Fig. 8. Cholesterol redistributes to lysosomes upon TAM and OHT treatment in scGT1 cells. scGT1 cells were treated with either rapamycin, TAM and OHT for 5 days and distribution of cholesterol was examined by filipin staining (in blue). An immunofluorescence assay with LAMP1 antibody (in green) was used to evaluate the presence of cholesterol in lysosomes. Note that upon TAM and OHT treatment, but not under rapamycin treatment or starvation, cholesterol partially accumulated in lysosomes (arrowheads in the 'insets'). Also, single-colour images of the insets are shown on the right.

cholesterol redistribution appears to affect PrP^{C} and PrP^{Sc} specifically because the subcellular localisation of the model GPI-anchored protein GFP-FR (Paladino et al., 2008) was not altered by TAM or OHT treatment (supplementary material Fig. S5).

Discussion

Prevailing models in the recent literature propose that the amount of protease-resistant, aggregated prion protein is maintained by a balance between PrP^{Sc} formation by conversion of native PrP^{C} and its destruction in lysosomes, which could be mediated by the autophagic pathway. In favour of this hypothesis, the appearance of multi-vesicular bodies and autophagic vacuoles has been reported in both prion-infected, neuronal cells in culture (Schätzl et al., 1997) and in brain biopsies from prion-infected patients (Liberski et al., 2008; Sikorska et al., 2004). Furthermore, stimulation of autophagy by chemical compounds such as rapamycin, lithium salts and trehalose was shown to reduce PrP^{Sc} in cultured cells (Aguib et al., 2009; Heiseke et al., 2009). These observations suggest a protective role for autophagy in prion infection and potentially identify the autophagic pathway as a target for therapeutic applications. Alternatively, it was proposed that autophagy may contribute to the spongiform changes that are a pathological hallmark of prion-affected brains, and may be activated by apoptosis (Liberski et al., 2008; Liberski and Jeffrey, 2004; Sikorska et al., 2004). These contradictory findings raised the question of the biological role of autophagy in prion infection and disease and prompted us to look more closely into the molecular interplay between autophagy, prion propagation, trafficking and clearance.

The first clue of an altered autophagic pathway in different neurodegenerative settings is the presence of an abnormal number of autophagosomes in affected neurons (Kegel et al., 2000; Nixon et al., 2005). In prion diseases an increased number of autophagosomes have been reported in infected neuronal cells and brain tissue (Liberski et al., 2008; Sikorska et al., 2004; Schätzl et al., 1997). Here we show that chronic scrapie infection enhances autophagic flux, but not autophagy per se, which is already active in neuronal cell culture (Fig. 1; supplementary material Fig. S1A,B) as previously shown in primary neurons (Mitra et al., 2009; Son et al., 2012). These results were in contrast to previous reports in which basal levels of autophagy could not be detected in non-infected N2a cells (Aguib et al., 2009; Heiseke et al., 2009). The most likely reason for this discrepancy was the different tool used in this study to monitor autophagy, namely, tandem fluorescent LC3 (tf-LC3) containing both GFP and RFP. Using this construct it is possible to distinguish autophagosomes from autolysosomes on the basis of the differential sensitivity of the green and red fluorophores to the acidic conditions in the phagolysosomal compartment (Kimura et al., 2009). In contrast, earlier studies reporting no basal autophagy in N2a cells were based only on observations of autophagosomes since the autolysosomes present were essentially invisible when using GFP–LC3 alone.

Although chronic scrapie infection increases autophagic flux, PrP^{Sc} is mostly absent from autophagic vesicles, even when lysosomal degradation is impaired (Fig. 3). This observation raised the possibility that PrP^{Sc} is not processed by the autophagic machinery. In fact, when Alexa-Fluor-546-labelled PrPSc was added to cells transfected with GFP–LC3 and analysed by live imaging we could observe a clear induction of autophagy but no colocalisation of Alexa-Fluor-546–PrP^{Sc} with LC3-decorated vesicles (supplementary material Movies 1–3). This suggests that PrP^{Sc} is able to escape autophagy during primary infection. Recently, similar observations were made in cells harbouring mutant Htt, in which cargo recognition failure by the autophagic pathway was detected (Li et al., 2010). One unanswered question from this study was: why is autophagy induced by prion infection despite its lack of involvement in its processing? It is possible that the presence of protein aggregates stimulates autophagic flux as a defensive response. However, prions, being membrane-bound proteins, may be able to elude recognition by the autophagic machinery by virtue of their sequestration within vesicles. In addition we found that autophagy could not be further enhanced in prion-infected cells with drugs such as rapamycin, TAM and OHT (supplementary material Fig. S1C,D; Fig. S2), which are effective autophagy inducers in non-infected cells as previously described [(de Medina et al., 2009) and data not shown].

Despite the lack of effect on autophagy we did observe increased PrP^{Sc} clearance upon TAM and OHT treatment (Fig. 2). This indicates that the mechanisms of PrP^{Sc} clearance by these compounds are probably independent of autophagy. This hypothesis was tested directly using a gene-silencing approach. Consistent with the microscopy data, inhibition of autophagy using Atg7 siRNA did not affect the ability of TAM and OHT to

reduce PrP^{Sc} content in infected cells (Fig. 4). Furthermore, prolonged knockdown of Atg7 did not lead to an accumulation of PrP^{Sc} above that in untreated cells, as would be expected if it was being degraded by autophagy. Overall these data argue against a major contribution of autophagy-mediated degradation in the regulation of PrP^{Sc} levels both in *de novo* or permanent infections and question the usefulness of autophagy as a target for therapy of prion diseases.

Ruling out a major involvement of autophagy in scrapie clearance raised the question of what was the mechanism by which TAM and OHT reduced PrP^{Sc} levels. We and others have previously shown that lipids, specifically cholesterol and sphingolipids, play a crucial role in PrP^{Sc} propagation and that changes in subcellular distribution of PrP by modulating lipid metabolism and trafficking, affect PrP^{Sc} levels in infected cells (Campana et al., 2005; Marijanovic et al., 2009; Lewis and Hooper, 2011; Taraboulos et al., 1995). Furthermore PrP^{C} and PrP^{Sc} have high affinity for membrane domains enriched in cholesterol and saturated lipids [rafts or detergent resistant microdomains (DRMs)] both *in vitro* and *in vivo* (Critchley et al., 2004; Galvan et al., 2005; Marijanovic et al., 2009; Sanghera et al., 2011). Interestingly, it has been shown that cholesterol levels regulate the distribution of PrP^{C} in different membrane domains (axons versus dendrites) in fully polarized primary neurons (Galvan et al., 2005). This could be due to the high sensitivity of lipid raft microdomains to cholesterol levels, as the authors speculate (Galvan et al., 2005), or to a direct effect of cholesterol levels on PrP localisation. The latter is supported by the fact that in polarized epithelial cells PrP^{C} is sorted to the basolateral membrane (Sarnataro et al., 2002), which is enriched in cholesterol compared with the apical membrane (Busche et al., 2002), and that perturbation of DRM association does not affect BL sorting (Sarnataro et al., 2002). Furthermore both PrP and PrP^{Sc} appear to be highly enriched in the recycling compartment (Marijanovic et al., 2009), which contains high cholesterol levels (Wüstner et al., 2002; Hao et al., 2002). Interestingly, although both TAM and OHT are inhibitors of cholesterol biosynthesis (de Medina et al., 2011; de Medina et al., 2004; de Medina et al., 2009), TAM has also been shown to inhibit the exit of cholesterol from lysosomes resulting in a lipid storage disease phenotype, characterized by the accumulation of cholesterol-laden late endosomes/lysosomes (Suárez et al., 2004). We observed a similar effect of both TAM and OHT on cholesterol trafficking in our cellular models (Fig. 8) with a substantial increase of cholesterol in lysosomes. Importantly, these treatments induced the redistribution of PrP^{Sc} and PrP^{C} towards lysosomes (Figs 5, 7), which could have an effect on both conversion and degradation of PrP^{Sc}. Indeed, in control conditions PrP^{C} and PrP^{Sc} are highly enriched in the endosomal recycling compartment where conversion occurs (Marijanovic et al., 2009). We have previously proposed that the high enrichment of cholesterol in these membranes (Wüstner et al., 2002; Hao et al., 2002) facilitates the encounter of PrP^{C} and PrP^{Sc} and the conversion process (Marijanovic et al., 2009). However, conditions that favour lysosomal degradation over endosomal recycling by re-routing PrP^{C} (the substrate of the conversion) from recycling endosomes to lysosomes, as occurs with TAM and OHT treatments, could reduce PrP^{Sc} conversion and should facilitate its elimination by the lysosomal system. If this is the case, the prediction would be that inhibition of lysosomal degradation should counteract the effect of OHT. Indeed, when we blocked lysosomal degradation using NH_4Cl in OHT-treated cells, higher levels of PrP^{Sc} were observed (Fig. 7). Consistent with the hypothesis that redistribution of cholesterol in lysosomes is a key event in the regulation of PrP trafficking towards this organelle, U18666A, a drug that induces a Niemann-Pick C cell (NPC) phenotype, similar to TAM treatment, with cholesterol accumulation in late endosomes/lysosomes (Lange et al., 2000) has been reported to accelerate PrP^{Sc} degradation. Of interest, this effect was counteracted by overexpression of Rab9 (Gilch et al., 2009), which has been shown to induce cholesterol efflux from lysosomes (Ganley and Pfeffer, 2006; Narita et al., 2005). Like U18666A, tamoxifen and its more potent derivative OHT are amphipathic weak bases. Therefore, it seems very likely that the effects observed are related to the amphipathic weak base properties and do not rely on the oestrogen-receptor-binding characteristics of tamoxifen. Also, it has been shown that changes related to lysosomal cholesterol accumulation as a result of NPC mutations or amphipathic weak base treatment alter the trafficking of many membrane components (Choudhury et al., 2004; Mukherjee and Maxfield, 2004; Rujoi et al., 2010). Therefore, although TAM represents a well-characterized, widely available pharmaceutical that may have

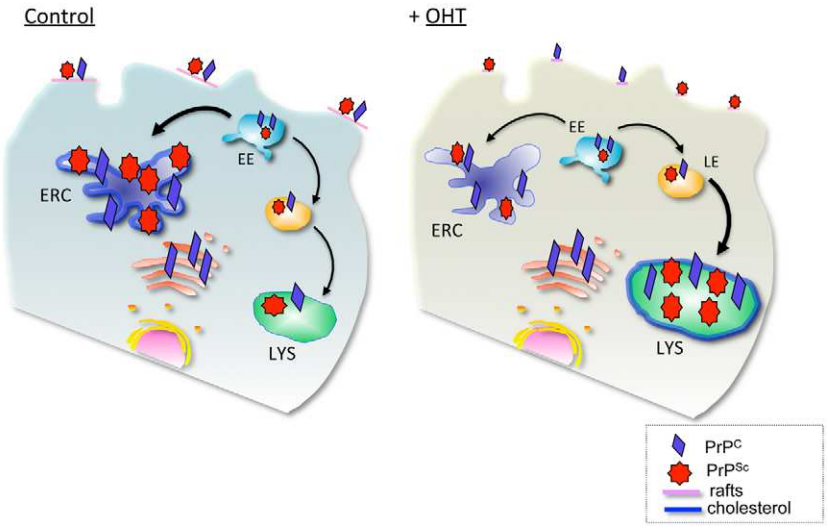

Fig. 9. Schematic presentation of PrP trafficking in infected cells and upon OHT treatment. In infected cells PrP^{C} and PrP^{Sc} interact at the plasma membrane in cholesterol-rich lipid domains called lipid rafts. Upon internalization, both PrP^{C} and PrP^{Sc} can recycle via the endosomal recycling compartment (ERC) or can be routed for degradation in lysosomes. Subcellular cholesterol distribution influences PrP^{Sc} trafficking in the endocytic pathway. In untreated, infected cells, the majority of PrP recycles through the cholesterol-rich ERC, supporting conversion of PrP^{C} to PrP^{Sc}. Treatment with 4-hydroxytamoxifen (OHT) induces cholesterol accumulation in enlarged late endosomes (LE). PrP^{Sc} production and degradation defines the cellular load of infectious prions. We propose that 4-hydroxytamoxifen-induced changes in PrP^{Sc} trafficking favour PrP^{Sc} degradation. EE, early endosomes; LYS, lysosomes.

applications as a broad-spectrum therapy for prion diseases, drugs sharing weak amphipathic bases properties with less selective biological effect than tamoxifen could be tested as possible candidates in the therapy for these diseases.

In conclusion, although autophagy is a well-known mechanism for directing aggregated proteins into lysosomes it appears that TAM and OHT induce the trafficking of prions to lysosomes in an autophagy-independent fashion. We therefore propose that by redirecting cholesterol to lysosomes these compounds alter the intracellular distribution of PrP^{C} and PrP^{Sc} along the endocytic pathway, thus shifting equilibrium towards PrP^{Sc} degradation (Fig. 9), which can be used as novel therapeutic approach for prion diseases.

Materials and Methods

Chemicals and antibodies

Rapamycin, TAM, OHT and Bafilomycin A1 were all purchased from Sigma. SAF32 and Sha31 anti-prion antibodies were purchased from SpiBio. Anti-tubulin monoclonal antibody and anti-ATG7 antibody were from Sigma. All the fluorescently labelled secondary antibodies, as well as Lysotracker® Green were purchased from Invitrogen (Molecular Probes). Anti-LAMP1 antibodies were purchased from BD Pharmingen™. Anti-LC3 monoclonal antibody, used for western blotting, was from nanoTools and anti-LC3 polyclonal antibody, used for immunofluorescence, was purchased from MBL International.

Fluorescently labelled PrP^{Sc} (Alexa-Fluor-546–PrP^{Sc}) was prepared as previously described (Gousset et al., 2009).

Cell lines

GT1-1 cells (a gift from Dr P. Mellon, University of California, San Diego, USA) were infected with the RML prion strain (a gift from Dr K. Korth, Heinrich Heine University, Dusseldorf, Germany). N2a cells and scN2a cells (infected with 22L prion strain) were provided by Dr K. Korth.

Non-infected and prion-infected GT1-1 and N2a cells were maintained in Dulbecco's modified Eagle's medium (DMEM; Invitrogen) supplemented with 10% fetal calf serum (FCS). CAD and scCAD (infected with 139A prion strain) were both gifts from Dr H. Laude (Institut National de la Recherche Agronomique, Jouy-en-Josas, France) and were cultured in Opti-MEM (Invitrogen) with addition of 10% FBS.

Plasmids, siRNAs and transfection procedures

The tandem fluorescently tagged (with both GFP and RFP) LC3 (Tf-LC3) and GFP-LC3 plasmids were a kind gift from Dr A. Ballabio [Telethon Institute of Genetis and Medicine (TIGEM), Naples, Italy] and Dr T. Yoshimori (Research Institute for Microbial Diseases, Osaka University, Osaka, Japan). Atg7 siRNA predesigned ON TARGETplus SMARTpool and siGENOME RISC-Free Control siRNA were both purchased from Dharmacon.

GT1-1 and scGT1 cells were transfected at 50% confluency using FuGENE6 (Roche Diagnostic) for DNA constructs according to manufacturer's protocol. To downregulate Atg7, 100 nM of the oligonucleotide was used with 10 µl of HiPerFect (Quiagen) per 60 mm dish. Hyperfect reagent was mixed with siRNA in DMEM without FBS, incubated for 10 minutes at room temperature and added to the cells.

Transfection of both non-infected and infected CAD and N2a cells with DNA constructs was done using Lipofectamine 2000 (Invitrogen), according to manufacturer's protocol.

When detection of PrP^{Sc} levels was performed, downregulation and overexpression of the proteins were maintained for a 5-day period. Therefore, in all the experiments siRNA and plasmids, except for pEGFP, were transfected twice (a second round of transfection was performed 3 days post-transfection).

Treatment of scGT1 and scN2a cells with different drugs

Rapamycin, TAM, OHT were reconstituted according to manufacturer's instructions. All the drugs were used in DMEM + 10% FCS at the final concentration of 2 µM for rapamycin, and 5 µM for TAM and OHT. During the 3- or 5-day treatment, medium containing the different drugs was changed every 2 days. A 5 M stock concentration of NH_4Cl from powder (Sigma) was prepared in sterile Ultra-pure MilliQ water.

When needed, Bafilomycin A1 or NH_4Cl (100 µM and 15 mM, respectively) were added to the rapamycin, TAM or OHT 5-day treatment for 2 days starting from the fourth day of the different treatments. For starvation treatment, cells where cultured in Earle's balanced salt solution (EBSS; Sigma) for 4 hours as previously described (Kimura et al., 2009).

Protein analysis by western blotting

Cells, grown in 60 mm dishes after the different treatments, were lysed in 500 µl of lysis buffer [0.5% Triton X-100, 0.5% deoxycholic acid (DOC), 100 mM NaCl, 10 mM Tris-HCl pH 8]. To analyse PrP^{Sc} levels, 250 µg of protein/lysate were treated with 5 µg proteinase K (PK) for 30 minutes at 37℃. This step allows the detection of PrP^{Sc} only, because of its partial resistance to PK (Prusiner et al., 1984). The protein content was then methanol precipitated overnight at −20℃ and centrifuged at 13,000 ***g*** for 30 minutes. After drying at 100℃, the pellet was resuspended and denatured in Laemmli buffer before SDS-PAGE and western blotting with the Sha31 anti-PrP antibody. All the other proteins, including total PrP, were analysed by western blotting from 20 or 40 µg of total lysate. HRP-conjugated secondary antibodies and ECL™ reagents from Amersham (GE Healthcare) were used for detection.

Immunofluorescence

For immunofluorescence analysis cells grown on coverslips in a 24-well plate for 3 days were carefully washed with PBS, fixed with 2% paraformaldehyde (PFA) for 30 minutes and permeabilised with 0.1% Triton X-100/PBS. A denaturation step with 6 M guanidine hydrochloride for 10 minutes was performed after permeabilisation to detect PrP^{Sc} in infected cells (Taraboulos et al., 1990), when needed. Cells were then blocked in 2% BSA/PBS, immunolabelled with primary and secondary antibodies and mounted with Aqua/Poly Mount (Polysciences).

In order to label endogenous LC3, cells were treated as previously described (Kimura et al., 2009).

When filipin staining was used, cells were fixed with 4% PFA for 60 minutes and blocked with 0.2% BSA/PBS. Filipin (250 µg/ml) was added to blocking solution and an additional 30 minute incubation was performed after incubation with secondary antibodies.

Fluorescence microscopy

Immunofluorescence micrographs were acquired using a high-resolution wide-field microscope Marianas (Intelligent Imaging Innovations) with a 63× oil objective. All Z-stacks were acquired with Z-steps of 0.27 µm. The auto-scaling (min/max) of signal detection was used to record only maximal signal intensities when PrP^{Sc} was analysed (Marijanovic et al., 2009).

In the experiments with live cells, CAD cells plated on ibidi dishes were either transfected with GFP-LC3 plasmid or incubated with LysoTracker (1:1000 dilution) for 30 minutes at 37℃ prior to be challenged with 1 µl/dish of sonicated Alexa-Fluor-546–PrP^{Sc}. Time-lapse movies were acquired with Biostation IM (from Nikon) and a wide-field microscope (Zeiss Axiovert 200M) controlled by Axiovision software.

Image processing and quantification

Raw data (both images and movies) were processed with ImageJ software. The constrained iterative algorithm in Slidebook 4.2 software (Intelligent Imaging Innovations) was used to deconvolve the images. Colocalisation was quantified by intensity correlation coefficient-based (ICCB) analysis using JACoP (Bolte and Cordelières, 2006). Statistical analysis of the correlation of the intensity values of both green and red pixels or blue and red pixels in dual-channel images was performed using Pearson's and Manders' coefficient and Van Steensel's approach (van Steensel et al., 1996).

Statistical analysis

All data were statistically validated by Student's *t*-test (unpaired two-tailed and single sample *t*-test). The differences were considered significant when $P<0.05$.

Acknowledgements

We would like to thank all the members of the Zurzolo Lab for helpful discussion.

Author contributions

C.Z. conceived and coordinated the project. L.M., Z.M., and D.B. planned, discussed and performed most of the experiments and analysed the data. A.C. helped with the experiments in PrPSc infected cells. Z.C. performed all the experiments to answer the referees comments and discussed the data. L.M., Z.M., D.B. and C.Z. wrote the manuscript. All authors discussed the results and manuscript text.

Funding

This work was supported by the European Union FP7 Priority [grant number 222887 to C.Z.]; by the Agence Nationale de Recherche [grant numbers: Priontraf ANR-09-BLAN-0122-01, and DISCover to C.Z., ANR 2009 NEUR 00203 to C.Z.]. L.M. was supported by a borsa di dottorato from the MIUR; Z.M. was supported by an Ile de France postdoctoral fellowship; D.B. was supported by a

postdoctoral fellowship from the Canadian Louis Pasteur Foundation.

Supplementary material available online at
http://jcs.biologists.org/lookup/suppl/doi:10.1242/jcs.114801/-/DC1

References

Aguib, Y., Heiseke, A., Gilch, S., Riemer, C., Baier, M., Schätzl, H. M. and Ertmer, A. (2009). Autophagy induction by trehalose counteracts cellular prion infection. *Autophagy* **5**, 361-369.

Bolte, S. and Cordelières, F. P. (2006). A guided tour into subcellular colocalization analysis in light microscopy. *J. Microsc.* **224**, 213-232.

Busche, R., Dittmann, J., Meyer zu Düttingdorf, H. D., Glockenthör, U., von Engelhardt, W. and Sallmann, H. P. (2002). Permeability properties of apical and basolateral membranes of the guinea pig caecal and colonic epithelia for short-chain fatty acids. *Biochim. Biophys. Acta* **1565**, 55-63.

Campana, V., Sarnataro, D. and Zurzolo, C. (2005). The highways and byways of prion protein trafficking. *Trends Cell Biol.* **15**, 102-111.

Caughey, B., Baron, G. S., Chesebro, B. and Jeffrey, M. (2009). Getting a grip on prions: oligomers, amyloids, and pathological membrane interactions. *Annu. Rev. Biochem.* **78**, 177-204.

Cherra, S. J., 3rd, Dagda, R. K. and Chu, C. T. (2010). Review: autophagy and neurodegeneration: survival at a cost? *Neuropathol. Appl. Neurobiol.* **36**, 125-132.

Choudhury, A., Sharma, D. K., Marks, D. L. and Pagano, R. E. (2004). Elevated endosomal cholesterol levels in Niemann-Pick cells inhibit rab4 and perturb membrane recycling. *Mol. Biol. Cell* **15**, 4500-4511.

Critchley, P., Kazlauskaite, J., Eason, R. and Pinheiro, T. J. T. (2004). Binding of prion proteins to lipid membranes. *Biochem. Biophys. Res. Commun.* **313**, 559-567.

de Medina, P., Payré, B. L., Bernad, J., Bosser, I., Pipy, B., Silvente-Poirot, S., Favre, G., Faye, J.-C. and Poirot, M. (2004). Tamoxifen is a potent inhibitor of cholesterol esterification and prevents the formation of foam cells. *J. Pharmacol. Exp. Ther.* **308**, 1165-1173.

de Medina, P., Silvente-Poirot, S. and Poirot, M. (2009). Tamoxifen and AEBS ligands induced apoptosis and autophagy in breast cancer cells through the stimulation of sterol accumulation. *Autophagy* **5**, 1066-1067.

de Medina, P., Paillasse, M. R., Ségala, G., Khallouki, F., Brillouet, S., Dalenc, F., Courbon, F., Record, M., Poirot, M. and Silvente-Poirot, S. (2011). Importance of cholesterol and oxysterols metabolism in the pharmacology of tamoxifen and other AEBS ligands. *Chem. Phys. Lipids* **164**, 432-437.

Galvan, C., Camoletto, P. G., Dotti, C. G., Aguzzi, A. and Ledesma, M. D. (2005). Proper axonal distribution of PrP(C) depends on cholesterol-sphingomyelin-enriched membrane domains and is developmentally regulated in hippocampal neurons. *Mol. Cell. Neurosci.* **30**, 304-315.

Ganley, I. G. and Pfeffer, S. R. (2006). Cholesterol accumulation sequesters Rab9 and disrupts late endosome function in NPC1-deficient cells. *J. Biol. Chem.* **281**, 17890-17899.

Gilch, S., Bach, C., Lutzny, G., Vorberg, I. and Schätzl, H. M. (2009). Inhibition of cholesterol recycling impairs cellular PrP(Sc) propagation. *Cell. Mol. Life Sci.* **66**, 3979-3991.

Gousset, K., Schiff, E., Langevin, C., Marijanovic, Z., Caputo, A., Browman, D. T., Chenouard, N., de Chaumont, F., Martino, A., Enninga, J. et al. (2009). Prions hijack tunnelling nanotubes for intercellular spread. *Nat. Cell Biol.* **11**, 328-336.

Hao, M., Lin, S. X., Karylowski, O. J., Wüstner, D., McGraw, T. E. and Maxfield, F. R. (2002). Vesicular and non-vesicular sterol transport in living cells. The endocytic recycling compartment is a major sterol storage organelle. *J. Biol. Chem.* **277**, 609-617.

Hara, T., Nakamura, K., Matsui, M., Yamamoto, A., Nakahara, Y., Suzuki-Migishima, R., Yokoyama, M., Mishima, K., Saito, I., Okano, H. et al. (2006). Suppression of basal autophagy in neural cells causes neurodegenerative disease in mice. *Nature* **441**, 885-889.

Heiseke, A., Aguib, Y., Riemer, C., Baier, M. and Schätzl, H. M. (2009). Lithium induces clearance of protease resistant prion protein in prion-infected cells by induction of autophagy. *J. Neurochem.* **109**, 25-34.

Heiseke, A., Aguib, Y. and Schatzl, H. M. (2010). Autophagy, prion infection and their mutual interactions. *Curr. Issues Mol. Biol.* **12**, 87-97.

Kabeya, Y., Mizushima, N., Ueno, T., Yamamoto, A., Kirisako, T., Noda, T., Kominami, E., Ohsumi, Y. and Yoshimori, T. (2000). LC3, a mammalian homologue of yeast Apg8p, is localized in autophagosome membranes after processing. *EMBO J.* **19**, 5720-5728.

Kegel, K. B., Kim, M., Sapp, E., McIntyre, C., Castaño, J. G., Aronin, N. and DiFiglia, M. (2000). Huntingtin expression stimulates endosomal-lysosomal activity, endosome tubulation, and autophagy. *J. Neurosci.* **20**, 7268-7278.

Kimura, S., Fujita, N., Noda, T. and Yoshimori, T. (2009). Monitoring autophagy in mammalian cultured cells through the dynamics of LC3. *Methods Enzymol.* **452**, 1-12.

Klionsky, D. J. and Emr, S. D. (2000). Autophagy as a regulated pathway of cellular degradation. *Science* **290**, 1717-1721.

Klionsky, D. J., Abeliovich, H., Agostinis, P., Agrawal, D. K., Aliev, G., Askew, D. S., Baba, M., Baehrecke, E. H., Bahr, B. A., Ballabio, A. et al. (2008). Guidelines for the use and interpretation of assays for monitoring autophagy in higher eukaryotes. *Autophagy* **4**, 151-175.

Komatsu, M., Waguri, S., Chiba, T., Murata, S., Iwata, J., Tanida, I., Ueno, T., Koike, M., Uchiyama, Y., Kominami, E. et al. (2006). Loss of autophagy in the central nervous system causes neurodegeneration in mice. *Nature* **441**, 880-884.

Lange, Y., Ye, J., Rigney, M. and Steck, T. (2000). Cholesterol movement in Niemann-Pick type C cells and in cells treated with amphiphiles. *J. Biol. Chem.* **275**, 17468-17475.

Lewis, V. and Hooper, N. M. (2011). The role of lipid rafts in prion protein biology. *Front. Biosci.* **16**, 151-168.

Li, X., Wang, C.-E., Huang, S., Xu, X., Li, X.-J., Li, H. and Li, S. (2010). Inhibiting the ubiquitin-proteasome system leads to preferential accumulation of toxic N-terminal mutant huntingtin fragments. *Hum. Mol. Genet.* **19**, 2445-2455.

Liberski, P. P. and Jeffrey, M. (2004). Tubulovesicular structures – the ultrastructural hallmark for transmissible spongiform encephalopathies or prion diseases. *Folia Neuropathol.* **42 Suppl. B**, 96-108.

Liberski, P. P., Brown, D. R., Sikorska, B., Caughey, B. and Brown, P. (2008). Cell death and autophagy in prion diseases (transmissible spongiform encephalopathies). *Folia Neuropathol.* **46**, 1-25.

Marijanovic, Z., Caputo, A., Campana, V. and Zurzolo, C. (2009). Identification of an intracellular site of prion conversion. *PLoS Pathog.* **5**, e1000426.

Mitra, S., Tsvetkov, A. S. and Finkbeiner, S. (2009). Single neuron ubiquitin-proteasome dynamics accompanying inclusion body formation in huntington disease. *J. Biol. Chem.* **284**, 4398-4403.

Mukherjee, S. and Maxfield, F. R. (2004). Lipid and cholesterol trafficking in NPC. *Biochim. Biophys. Acta* **1685**, 28-37.

Narita, K., Choudhury, A., Dobrenis, K., Sharma, D. K., Holicky, E. L., Marks, D. L., Walkley, S. U. and Pagano, R. E. (2005). Protein transduction of Rab9 in Niemann-Pick C cells reduces cholesterol storage. *FASEB J.* **19**, 1558-1560.

Nixon, R. A., Wegiel, J., Kumar, A., Yu, W. H., Peterhoff, C., Cataldo, A. and Cuervo, A. M. (2005). Extensive involvement of autophagy in Alzheimer disease: an immuno-electron microscopy study. *J. Neuropathol. Exp. Neurol.* **64**, 113-122.

Paladino, S., Lebreton, S., Tivodar, S., Campana, V., Tempre, R. and Zurzolo, C. (2008). Different GPI-attachment signals affect the oligomerisation of GPI-anchored proteins and their apical sorting. *J. Cell Sci.* **121**, 4001-4007.

Prusiner, S. B. (1984). Prions. *Sci. Am.* **251**, 50-59.

Prusiner, S. B. (1998). Prions. *Proc. Natl. Acad. Sci. USA* **95**, 13363-13383.

Qadir, M. A., Kwok, B., Dragowska, W. H., To, K. H., Le, D., Bally, M. B. and Gorski, S. M. (2008). Macroautophagy inhibition sensitizes tamoxifen-resistant breast cancer cells and enhances mitochondrial depolarization. *Breast Cancer Res. Treat.* **112**, 389-403.

Rubinsztein, D. C., Gestwicki, J. E., Murphy, L. O. and Klionsky, D. J. (2007). Potential therapeutic applications of autophagy. *Nat. Rev. Drug Discov.* **6**, 304-312.

Rujoi, M., Pipalia, N. H. and Maxfield, F. R. (2010). Cholesterol pathways affected by small molecules that decrease sterol levels in Niemann-Pick type C mutant cells. *PLoS ONE* **5**, e12788.

Samaddar, J. S., Gaddy, V. T., Duplantier, J., Thandavan, S. P., Shah, M., Smith, M. J., Browning, D., Rawson, J., Smith, S. B., Barrett, J. T. et al. (2008). A role for macroautophagy in protection against 4-hydroxytamoxifen-induced cell death and the development of antiestrogen resistance. *Mol. Cancer Ther.* **7**, 2977-2987.

Sanghera, N., Correia, B. E. F. S., Correia, J. R. S., Ludwig, C., Agarwal, S., Nakamura, H. K., Kuwata, K., Samain, E., Gill, A. C., Bonev, B. B. et al. (2011). Deciphering the molecular details for the binding of the prion protein to main ganglioside GM1 of neuronal membranes. *Chem. Biol.* **18**, 1422-1431.

Sarnataro, D., Paladino, S., Campana, V., Grassi, J., Nitsch, L. and Zurzolo, C. (2002). PrPC is sorted to the basolateral membrane of epithelial cells independently of its association with rafts. *Traffic* **3**, 810-821.

Schätzl, H. M., Laszlo, L., Holtzman, D. M., Tatzelt, J., DeArmond, S. J., Weiner, R. I., Mobley, W. C. and Prusiner, S. B. (1997). A hypothalamic neuronal cell line persistently infected with scrapie prions exhibits apoptosis. *J. Virol.* **71**, 8821-8831.

Shyng, S. L., Huber, M. T. and Harris, D. A. (1993). A prion protein cycles between the cell surface and an endocytic compartment in cultured neuroblastoma cells. *J. Biol. Chem.* **268**, 15922-15928.

Sikorska, B., Liberski, P. P., Giraud, P., Kopp, N. and Brown, P. (2004). Autophagy is a part of ultrastructural synaptic pathology in Creutzfeldt-Jakob disease: a brain biopsy study. *Int. J. Biochem. Cell Biol.* **36**, 2563-2573.

Son, J. H., Shim, J. H., Kim, K. H., Ha, J. Y. and Han, J. Y. (2012). Neuronal autophagy and neurodegenerative diseases. *Exp. Mol. Med.* **44**, 89-98.

Suárez, Y., Fernández, C., Gómez-Coronado, D., Ferruelo, A. J., Dávalos, A., Martínez-Botas, J. and Lasunción, M. A. (2004). Synergistic upregulation of low-density lipoprotein receptor activity by tamoxifen and lovastatin. *Cardiovasc. Res.* **64**, 346-355.

Sunyach, C., Jen, A., Deng, J., Fitzgerald, K. T., Frobert, Y., Grassi, J., McCaffrey, M. W. and Morris, R. (2003). The mechanism of internalization of glycosylphosphatidylinositol-anchored prion protein. *EMBO J.* **22**, 3591-3601.

Taraboulos, A., Serban, D. and Prusiner, S. B. (1990). Scrapie prion proteins accumulate in the cytoplasm of persistently infected cultured cells. *J. Cell Biol.* **110**, 2117-2132.

Taraboulos, A., Scott, M., Semenov, A., Avrahami, D., Laszlo, L. and Prusiner, S. B. (1995). Cholesterol depletion and modification of COOH-terminal targeting sequence of the prion protein inhibit formation of the scrapie isoform. *J. Cell Biol.* **129**, 121-132.

van Steensel, B., van Binnendijk, E. P., Hornsby, C. D., van der Voort, H. T., Krozowski, Z. S., de Kloet, E. R. and van Driel, R. (1996). Partial colocalization of glucocorticoid and mineralocorticoid receptors in discrete compartments in nuclei of rat hippocampus neurons. *J. Cell Sci.* **109**, 787-792.

Wong, E. and Cuervo, A. M. (2010). Autophagy gone awry in neurodegenerative diseases. *Nat. Neurosci.* **13**, 805-811.

Wüstner, D., Herrmann, A., Hao, M. and Maxfield, F. R. (2002). Rapid nonvesicular transport of sterol between the plasma membrane domains of polarized hepatic cells. *J. Biol. Chem.* **277**, 30325-30336.